AFRL-PR-WP-TR-2001-2024

ANALYSIS OF SIMULATED AIRCRAFT LIGHTNING STRIKES AND THEIR ELECTROMAGNETIC EFFECTS

Major James M. Gruden
Lawrence C. Walko
Daniel L. Schweickart
John C. Horwath
Gary L. Webb

AFRL/PRPS
1950 5TH Street, Bldg. 450
Wright-Patterson AFB, OH 45433-7251

FEBRUARY 2001

FINAL REPORT FOR PERIOD JULY 1995 - JULY 1997

20010405 044

NOTICE

USING GOVERNMENT DRAWINGS, SPECIFICATIONS, OR OTHER DATA INCLUDED IN THIS DOCUMENT FOR ANY PURPOSE OTHER THAN GOVERNMENT PROCUREMENT DOES NOT IN ANY WAY OBLIGATE THE US GOVERNMENT. THE FACT THAT THE GOVERNMENT FORMULATED OR SUPPLIED THE DRAWINGS, SPECIFICATIONS, OR OTHER DATA DOES NOT LICENSE THE HOLDER OR ANY OTHER PERSON OR CORPORATION; OR CONVEY ANY RIGHTS OR PERMISSION TO MANUFACTURE, USE, OR SELL ANY PATENTED INVENTION THAT MAY RELATE TO THEM.

THIS REPORT IS RELEASABLE TO THE NATIONAL TECHNICAL INFORMATION SERVICE (NTIS). AT NTIS, IT WILL BE AVAILABLE TO THE GENERAL PUBLIC, INCLUDING FOREIGN NATIONS.

THIS TECHNICAL REPORT HAS BEEN REVIEWED AND IS APPROVED FOR PUBLICATION.

JAMES M. GRUDEN, Maj, USAFR
Power Systems Branch
Power Division

LAWRENCE C. WALKO
Power Systems Branch
Power Division

JERRY E. BEAM
Acting Chief
Power Division

Do not return copies of this report unless contractual obligations or notice on a specific document requires its return.

REPORT DOCUMENTATION PAGE

Public reporting burden for this collection of information is estimated to average 1 hour per response, including the time for reviewing instructions, searching existing data sources, gathering and maintaining the data needed, and completing and reviewing this collection of information. Send comments regarding this burden estimate or any other aspect of this collection of information, including suggestions for reducing this burden to Washington Headquarters Services, Directorate for Information Operations and Reports, 1215 Jefferson Davis Highway, Suite 1204, Arlington, VA 22202-4302, and to the Office of Management and Budget, Paperwork Reduction Project (0704-0188), Washington, DC 20503

1. AGENCY USE ONLY (Leave blank)	2. REPORT DATE February 2001	3. REPORT TYPE AND DATES COVERED Final July 1995 - July 1997	

4. TITLE AND SUBTITLE
Analysis of Simulated Aircraft Lightning Strikes and Their Electromagnetic Effects

5. FUNDING NUMBERS
C N/A
PE 62203F
PR 3145
TA 32
WU 29

6. AUTHOR(S)
Major James M. Gruden, Lawrence C. Walko, Daniel L. Schweickart,
John C. Horwath, Gary L. Webb

7. PERFORMING ORGANIZATION NAME(S) AND ADDRESS(ES)

AFRL/PRPS
1950 5TH Street, Bldg. 450
Wright-Patterson AFB, OH 45433-7251

8. PERFORMING ORGANIZATION REPORT NUMBER
AFRL-PR-WP-TR-2001-2024

9. SPONSORING / MONITORING AGENCY NAME(S) AND ADDRESS(ES)

Propulsion Directorate
Air Force Research Laboratory
Air Force Materiel Command
Wright-Patterson Air Force Base, OH 45433-7251
POC: Daniel L. Schweickart, AFRL/PRPS, (937) 255-9189

10. SPONSORING / MONITORING AGENCY REPORT NUMBER
AFRL-PR-WP-TR-2001-2024

11. SUPPLEMENTARY NOTES

12a. DISTRIBUTION / AVAILABILITY STATEMENT

Approved for public release; distribution unlimited.

12b. DISTRIBUTION CODE

13. ABSTRACT (Maximum 200 Words)

To survive the intense electromagnetic fields associated with a lightning strike, proper design of aircraft electrical control systems requires knowledge of the transient current pulse associated with a lightning strike. This report summarizes in-house testing of low-level (less than 20 kA) current pulses on a 32-foot long aluminum cylinder simulating an aircraft fuselage. The test circuit consists of a capacitor bank, the aluminum cylinder and a coaxial return path of 16 wires that reconnects the end of the cylinder to the capacitor bank. Areas of investigation included magnetic field mapping along various areas of the cylinder, with and without access panels, as well as different panel materials. The effects on circuits internal to the cylinder are also evaluated.

Using a magnetic field loop sensor, three-dimensional magnetic field plots are generated that depict how the magnetic field along the surface of the cylinder is distorted when it approaches an opening (access panel removed) along the surface of the cylinder. These plots identify the critical locations of the peak magnetic fields. Diffusion effects are also evaluated as the opening is relocated toward the end of the cylinder. Finally, induced currents on circuits internal to the cylinder are recorded and measured.

14. SUBJECT TERMS,

Lightning Strike, Electromagnetic Fields, Electromagnetic Effects, Aircraft.

15. NUMBER OF PAGES
28

16. PRICE CODE

17. SECURITY CLASSIFICATION OF REPORT Unclassified	18. SECURITY CLASSIIFICATION OF THIS PAGE Unclassified	19. SECURITY CLASSIFICATION OF ABSTRACT Unclassified	20. LIMITATION OF ABSTRACT SAR

Table of Contents

List of Figures

List of Tables

1.0 Introduction

Lightning strikes on aircraft cause many problems ranging from external structural damage to internal electrical control systems failures. The structural damage may affect a wing or control surface or merely result in burn marks on the skin of the aircraft requiring standard maintenance and repair procedures. Within the aircraft, the transient electromagnetic fields associated with a lightning strike can render sophisticated electronic avionics, navigation, and weapon systems ineffective to the point where the aircraft's mission can not be accomplished.

Over the years, much research has been conducted to better understand the nature of lightning, including its origin, stored energy levels, and discharge characteristics. The best defense against aircraft lightning strikes is to avoid them completely or maintain a "safe distance" from thunder storm clouds. Since these conditions can not always be met and because aircraft parked on the ground are also subject to lightning strikes, it quickly becomes evident that design strategies must be developed to "harden" the aircraft both physically and electronically to minimize any lightning strike damage.

To optimize effective designs, engineers need to understand the phenomena associated with the lightning strike as it attaches to the aircraft. Due to the strike, a current pulse may traverse the fuselage and generate an intense electromagnetic field within the aircraft before the pulse exits. This scenario defines the threat to electrical subsystems within the fuselage and drives the specific requirements and costs associated with appropriate EM countermeasures.

One way to acquire accurate data regarding the interaction between lightning and an aircraft is to instrument an aircraft with electromagnetic sensors, fly the aircraft near a storm cloud and monitor and record the electric and magnetic field changes both externally and internally to the aircraft. The advantage of this type of testing is that the data is "real" and only limited by sensor technology and data acquisition schemes. The obvious disadvantage is the risk the crew and aircraft are subjected to while acquiring the data. Additional limitations include the costs of undertaking missions that are dependent on weather conditions and specific geographic

areas. Also, the acquired data is specific to the particular aircraft flying the mission and is "biased" by the aircraft's structural profile, fuselage material, and internal construction.

A cost effective and safer alternative approach is to simulate the attachment of a lightning strike to a mock fuselage in a laboratory or test facility where conditions are controlled. By this method, lives and aircraft are not at risk and test scheduling is not governed by the weather conditions or geographic location. During simulated lightning strike tests, electromagnetic fields created by the current pulse traveling down the mock fuselage are safely monitored and analyzed at a lower power level to define the internal threat to electrical subsystems within the aircraft. The results can then be extrapolated to higher level lightning strikes to predict failure modes on specific aircraft in today's Air Force inventory.

This technical report provides an overview of simulated "low-level" lightning strike tests conducted in the High Power Test Facility at the Air Force Research Laboratory's Propulsion Directorate located at Wright-Patterson Air Force Base, OH. The term "low-level" refers to the amplitude of the simulated lightning stroke return current pulse. This current pulse is at the low end of the typical lightning amplitude distribution experienced in natural events, i.e. <20 kA in this investigation. The report begins with a description of the electrical circuit, test hardware, instrumentation, data acquisition system and the current pulse that simulates the low-level lightning strike. Using 3-D and 2-D field mapping plots, the report then illustrates various magnetic field profiles along the simulated fuselage and the effects of different fuselage panel materials. A small investigation is also conducted on the magnetic field effects of basic circuits internal to the fuselage. The report closes with conclusions and recommendations for additional testing.

2.0 Test Set-Up

2.1 Capacitor Bank and Circuit

A high current pulse generator was used to simulate the lightning return stroke. The generator consisted of two 8 μF capacitor banks in series. Each capacitor bank consisted of eight 4 μF capacitors in a series-parallel arrangement (Figure 1). [1] The 8 μF capacitor banks were charged in parallel to 100 kV$_{max}$ by a DC power supply through closed charging switches. When the desired charging voltage was reached, the charging switches were pneumatically opened to isolate the capacitor banks. The two capacitor banks then discharged in series through a pneumatically controlled spherical electrode resulting in a maximum energy level of 80 kilojoules.
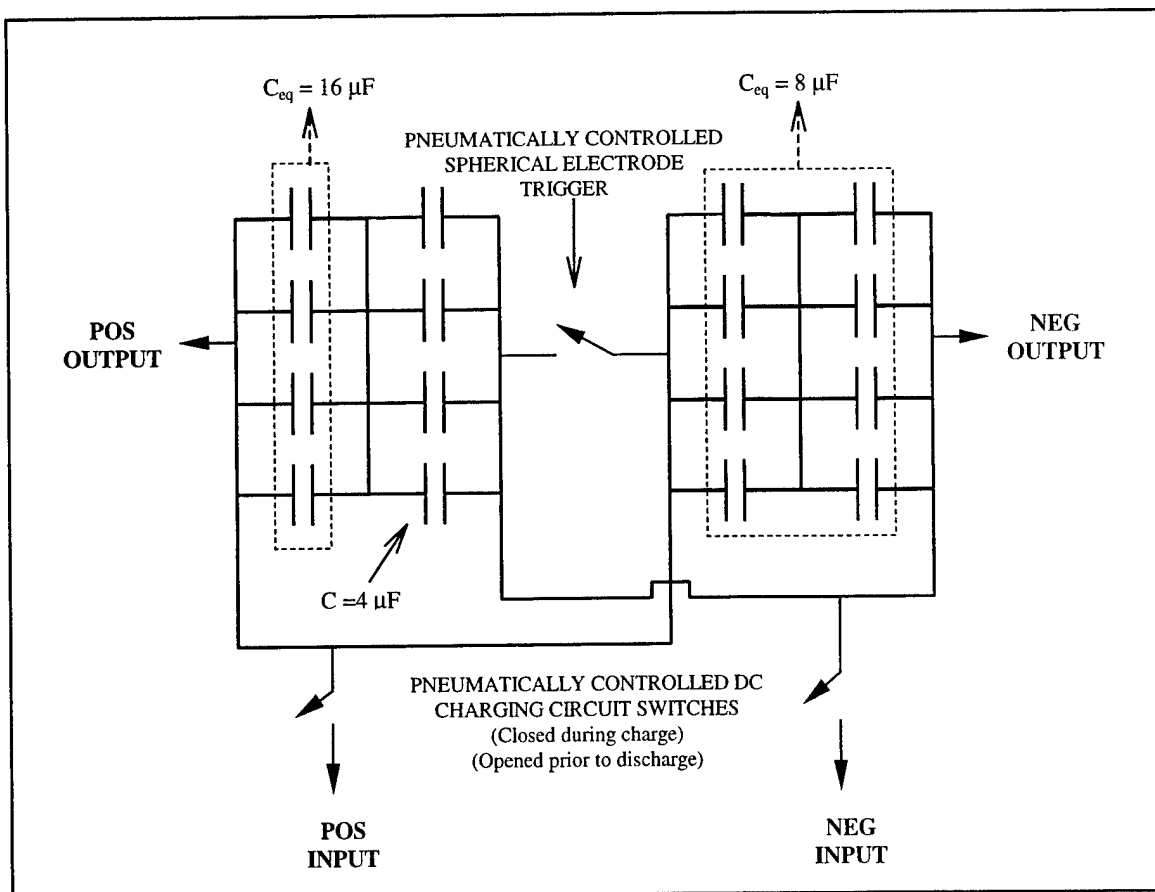
Figure 1. Capacitor Bank Configuration

The output current pulse of the capacitor bank was an overdamped sinusoid. Its characteristic wave shape was determined primarily by the capacitance of the capacitor bank (C_{tot}= 4 μF), the inductance of the capacitor bank (2 μH), and the resistance of the damping resistor (5 Ω) attached to the capacitor bank's output terminal. Figure 2 shows a typical capacitor bank current pulse used to simulate a low-level lightning strike.
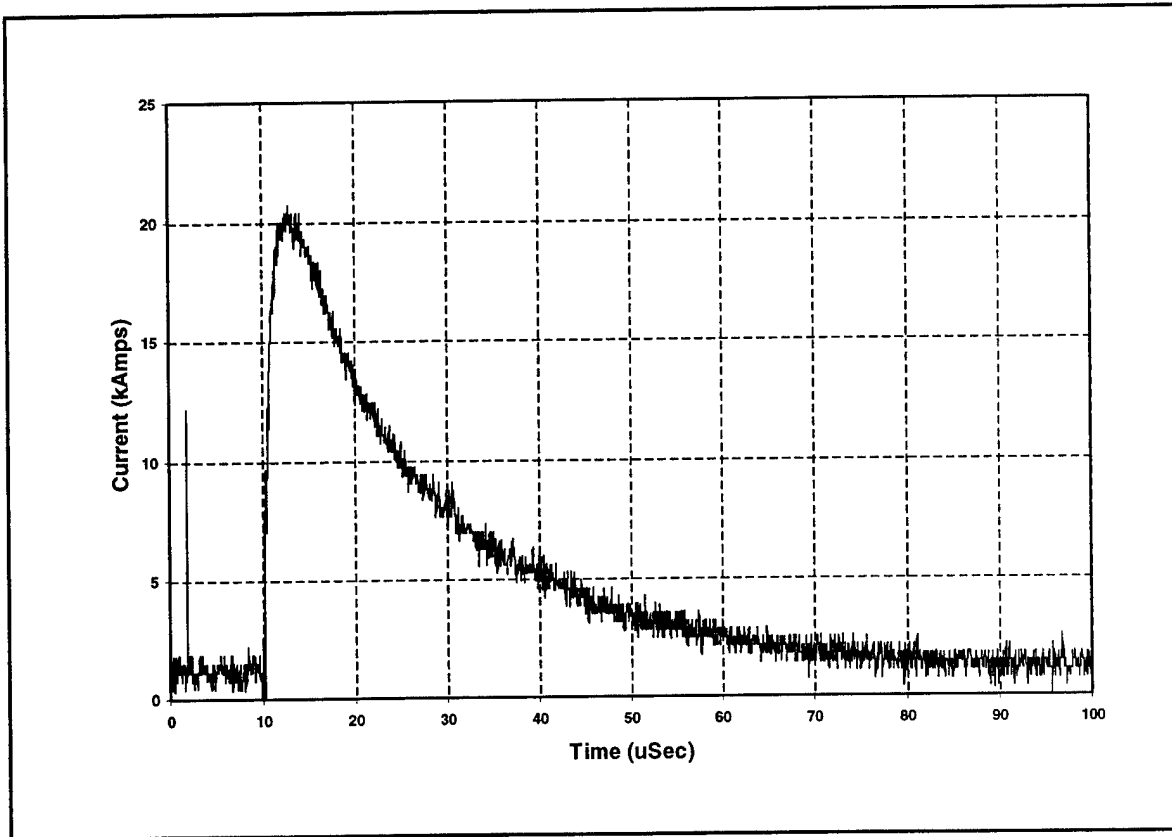
Figure 2. Typical Current Pulse

The output of the capacitor bank was connected directly to an aluminum cylinder simulating an aircraft fuselage, through four 10 AWG wires equally spaced around the perimeter of the front endplate of the aluminum cylinder. After axially traveling the full length of the aluminum cylinder, the current pulse returned to the capacitor bank via sixteen 16 AWG wires connected between to the rear endplate and the capacitor bank. The wires were arranged in a

4

coaxial configuration approximately four-and-a-half feet away from the cylinder to minimize any stray electromagnetic fields and encourage a more uniform current distribution in the cylinder.

2.2 Aluminum Cylinder

A cylinder made from 1/8 inch thick 6061-T4 aluminum is used to simulate the basic geometry of an aircraft fuselage. The cylinder is approximately 38 inches in diameter and consisted of four sections each eight foot in length for a total length of 32 feet. The cylinder is supported from the floor by three wooden stanchions that placed the centerline of the cylinder about five feet above the floor (Figure 3). [2]

Aluminum Cylinder (32 foot long)

Capacitor Banks (8 μF, 40 kJ each)

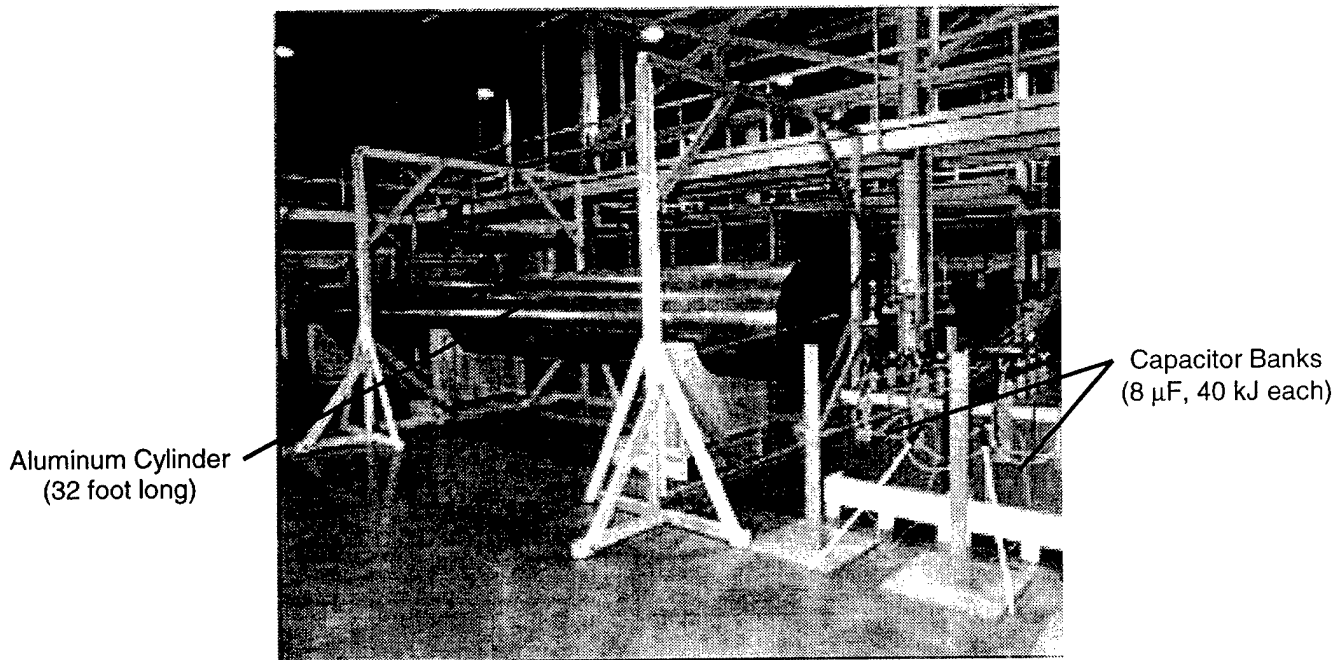**Figure 3.** Aluminum Cylinder and Capacitor Bank

To simulate aircraft access panels, sixteen 24 inch X 15 inch panels are located along the full length of the cylinder. These panels not only serve as access points for locating instrumentation but also serve to demonstrate the effects of seams in the aircraft's skin where electromagnetic fields could possibly penetrate. Panels fabricated from copper, brass screen and

aluminum screen are also used in place of the aluminum panels and tested to determine their effects on electromagnetic fields penetrating into the aluminum cylinder.

2.3 Data Acquisition and Instrumentation

Data was acquired using a fiber optics data link with a response from DC to 150 MHz. The capacitor bank current was monitored through a 10,000:1 current viewing resistor attached to a current transformer made by T & M Research Products, Inc. (Model CT23.9-500-10-100) with a 0.31 - 300 MHz bandwidth. The magnetic fields were monitored using loop sensors while surface currents were tracked with a surface mounted B-dot ground plane sensor manufactured by EG&G (Model MCL-S7A(R)).

The sensor signals were transmitted through fiber optic cables (SIV/30) using a Meret Inc. battery operated transmitter module to a shielded room where they were received and either integrated (B-dot signals) or sent directly to a LeCroy 7200 Precision Digital Oscilloscope for analysis and storage (Figure 4).
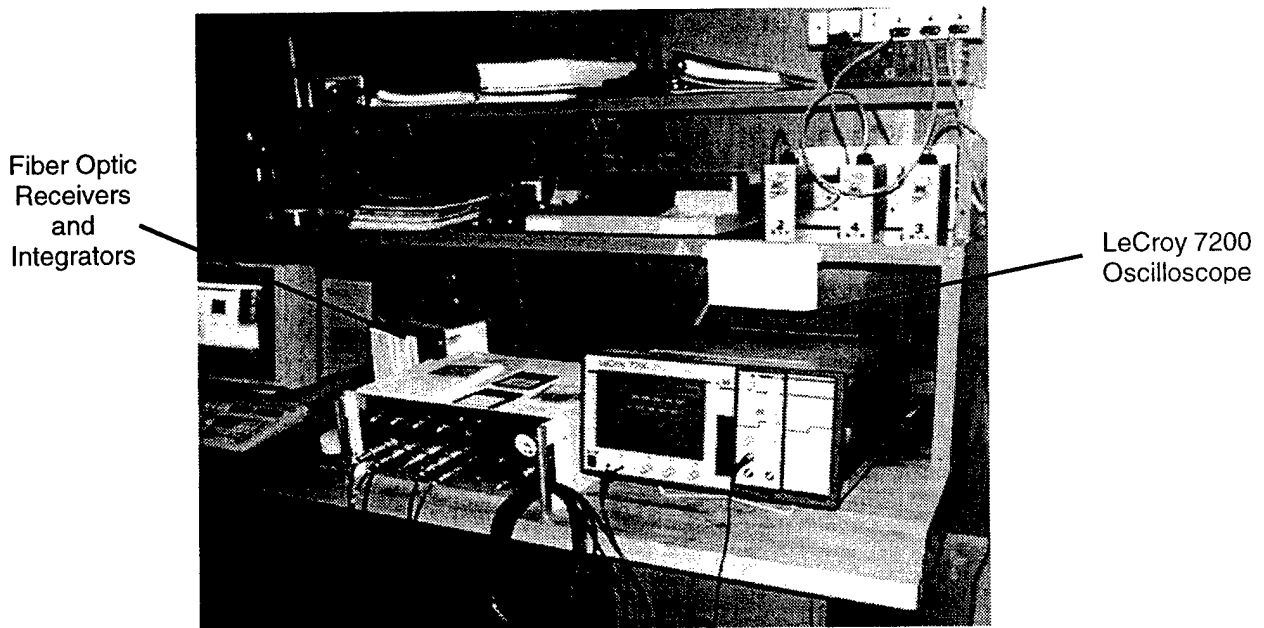

Fiber Optic Receivers and Integrators

LeCroy 7200 Oscilloscope

Figure 4. Data Acquisition in Shielded Room

The primary reason for conducting these simulated lightning strike tests was to track and record the resulting magnetic fields at different locations inside the aluminum cylinder as the current pulse from the capacitor bank traveled down the length of the simulated aircraft fuselage. Since the magnetic fields of primary concern were internal to the "closed" cylinder, a scheme was devised to locate a magnetic field loop sensor at various positions within the cylinder.

The scheme consisted of a long fiberglass pole running through the center axis of the cylinder with internal bearing supports appropriately spaced along the pole's length. Perpendicular to the pole was a smaller fiberglass arm that was used to mount the magnetic field loop sensor (Figure 5). Since the centrally located pole protruded through the ends of the cylinder, it could be rotated to obtain various angular positions for the sensor. It could also be moved along the axis of the cylinder to obtain various axial sensor positions. The location of the sensor on the smaller arm provided a range of radial positions as well. This sensor-positioning scheme enabled magnetic field "mapping" inside the cylinder where panels had been removed or reconfigured. It also saved a considerable amount of time when repositioning the sensor since the panels, which each had 38 screws fastening them to the cylinder, did not have to be unscrewed and then re-screwed into the cylinder each time the sensor needed to be repositioned.

Figure 5. Magnetic Field Loop Sensor

To track sensor position during a test, a grid system was established for the cylinder's removable access panels that identified the position of the sensor during data acquisition (Figure 6). Each of the access panels was numbered 1 through 16 starting at the cylinder's end closest to the capacitor bank. We also investigated four types of panel materials in one area of the cylinder. The "materials" included aluminum, copper, brass screen and air (no panel).
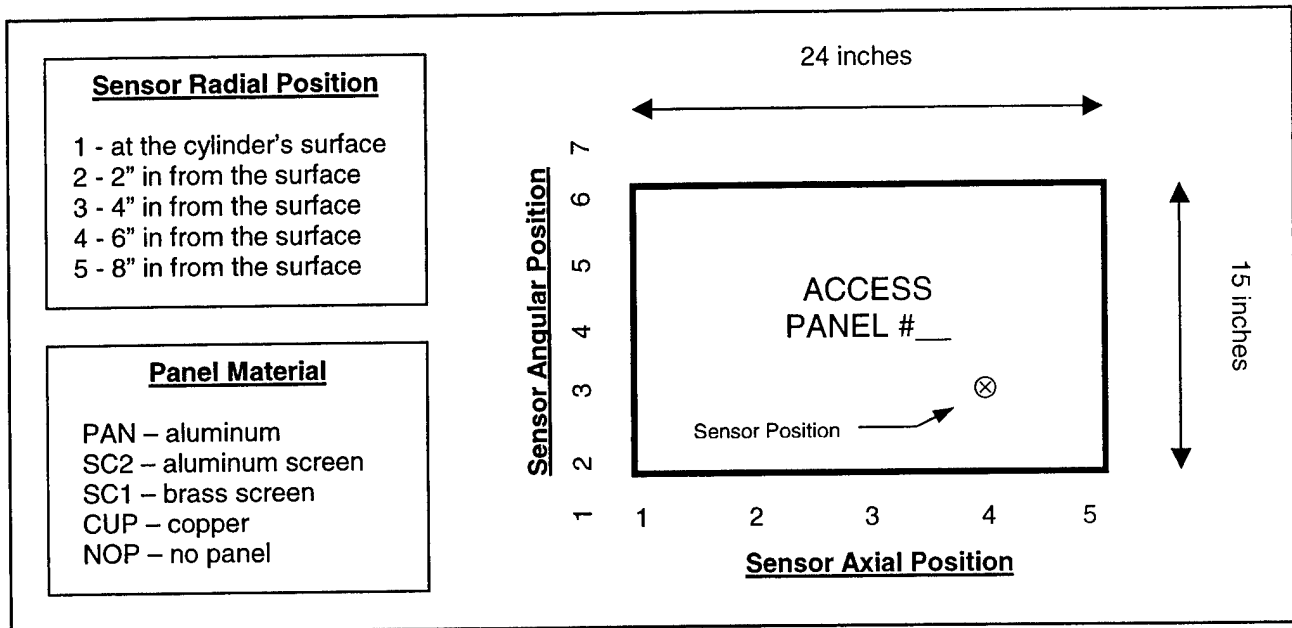
Figure 6. Sensor Location and Panel Material Identification

To assist in managing data files, each test run was assigned a file name with the following format: X_##_YYY.###. The "X" represented the type of sensor being used, i.e. S = H-Field loop sensor, I = current sensor, etc. "##" identified the cylinder's panel number where the test occurred. "YYY" represented the panel's material (Figure 6). "###" identified the axial, angular, and radial positions respectively of the loop sensor. As an example, file S_03_PAN.433 contained the signal from the loop sensor (S) located 4" below the surface of Panel #03 (material: aluminum). The sensor's axial and angular position are located in Figure 6 with the "⊗" symbol.

8

Figure 7 shows the Test Engineer installing copper access Panel #03 on the aluminum cylinder as preparations are made to run a test.
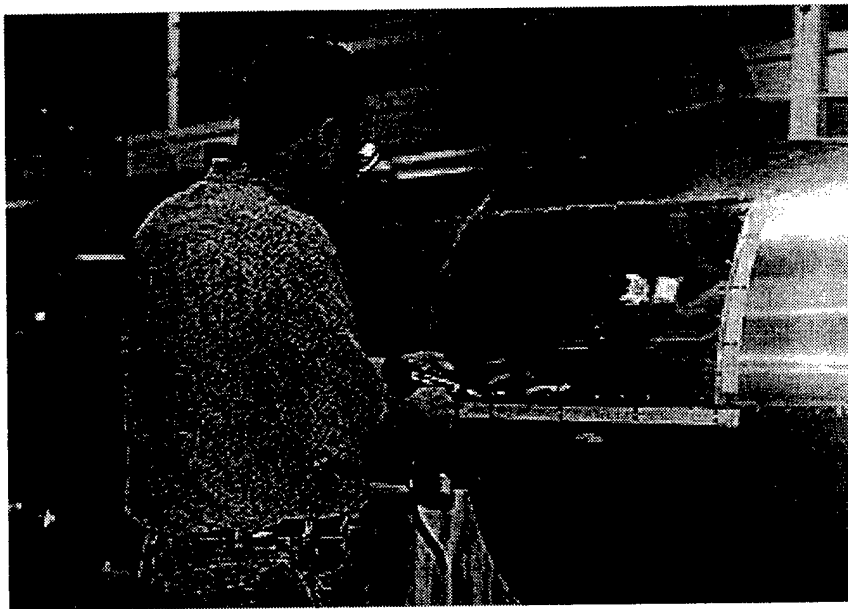
Figure 7. Installation of Copper Access Panel #03

To ensure the test site was safe to conduct a test, a closed circuit video camera was installed to monitor the area surrounding the capacitor bank and aluminum cylinder. The TV screen for the video camera was placed in the screen room where the test sequence was initiated. In addition to the area being roped off, flashing lights and audible buzzers were activated to warn nearby personnel that the test would soon begin or was already in progress.

3.0 Results

3.1 Magnetic Field Variations

Initially, our testing focused around the area of access Panel #03. This area was nominally five feet from the end of the aluminum cylinder closest to the capacitor bank. We removed the access panel and mapped the magnetic field's magnitude and polarity as the loop sensor was moved to 35 different grid positions defined in Figure 6 (refer to page 8). The sensor remained in radial position #1, i.e. at the cylinder's surface during the field mapping. The capacitor bank was discharged 35 times with a relatively consistent peak current of approximately 3.5 kA. Before each shot, the magnetic field sensor was moved to the next grid location to monitor the transient response of the magnetic field in the new location.

Figure 8 shows a 3-D contour map of the magnetic field's magnitude and polarity fluctuations as the sensor was moved to the various 35 grid locations.
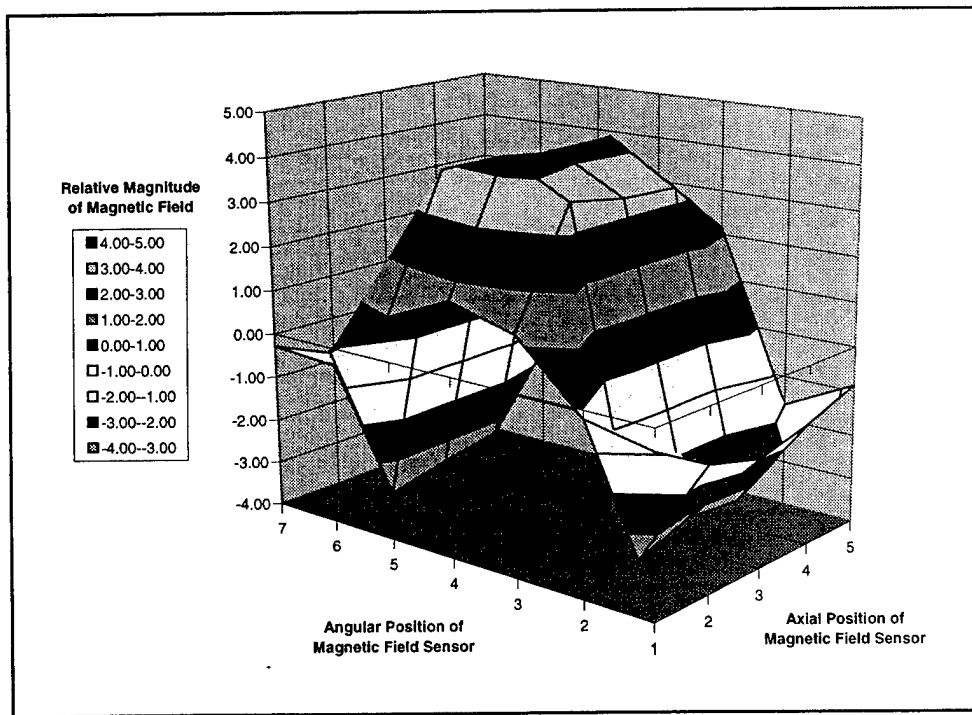

Figure 8. Relative Magnitude of Magnetic Field Across Panel #03 without the Panel in Place (Open)

Figure 9 provides the details of how a portion of the magnetic field mapping of Figure 8 was accomplished. The capacitor bank's discharge current is shown in the top left insert. The remaining seven plots show the transient nature of the magnetic field sensor's integrated output as it tracks the current pulse from the capacitor bank. The sample plots below show the magnetic field variations as the sensor was rotated in seven equal steps from the bottom center (Sensor Position 311) to the top center (Sensor Position 371) of Panel #03's opening. The peak value of each magnetic field plot was then used to generate the 3-D contour plot of Figure 8.
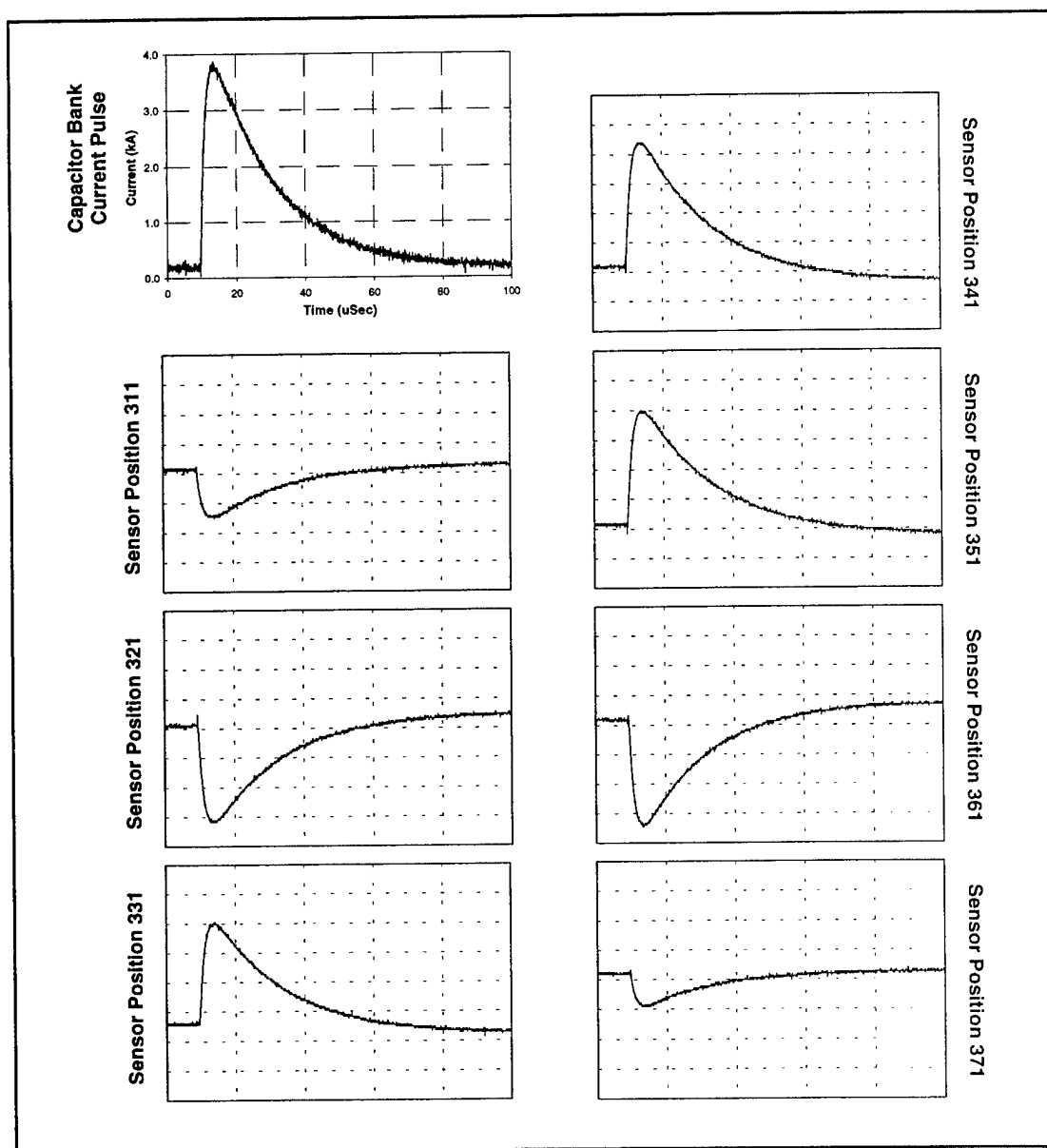

Figure 9. Magnetic Field Traces as the Loop Sensor is Rotated
from the Bottom Center to the Top Center of Panel #03

The following insights are gained from reviewing Figure 8 and Figure 9. A maximum "negative" magnetic field is found along the top and bottom edge of the opening. As the magnetic field loop sensor is rotated toward the center of the opening, the polarity of the field reverses and a maximum "positive" magnetic field occurs. Keep in mind that the magnetic field loop sensor remained at a constant radial distance from the main axis of the cylinder as it was rotated to all 35 positions to obtain the 3-D contour mapping. The sensor's radial position was adjacent to the "skin" of the simulated aircraft fuselage.

A similar magnetic field contour mapping was done on the cylinder's end opposite the capacitor bank (Panel #14). This area was nominally five feet away from the end of the cylinder where the coaxial return path wires were connected. Figure 10 shows the magnetic field contour map for the area of Panel #14 with the panel removed and a capacitor bank current of 3.3 kA.
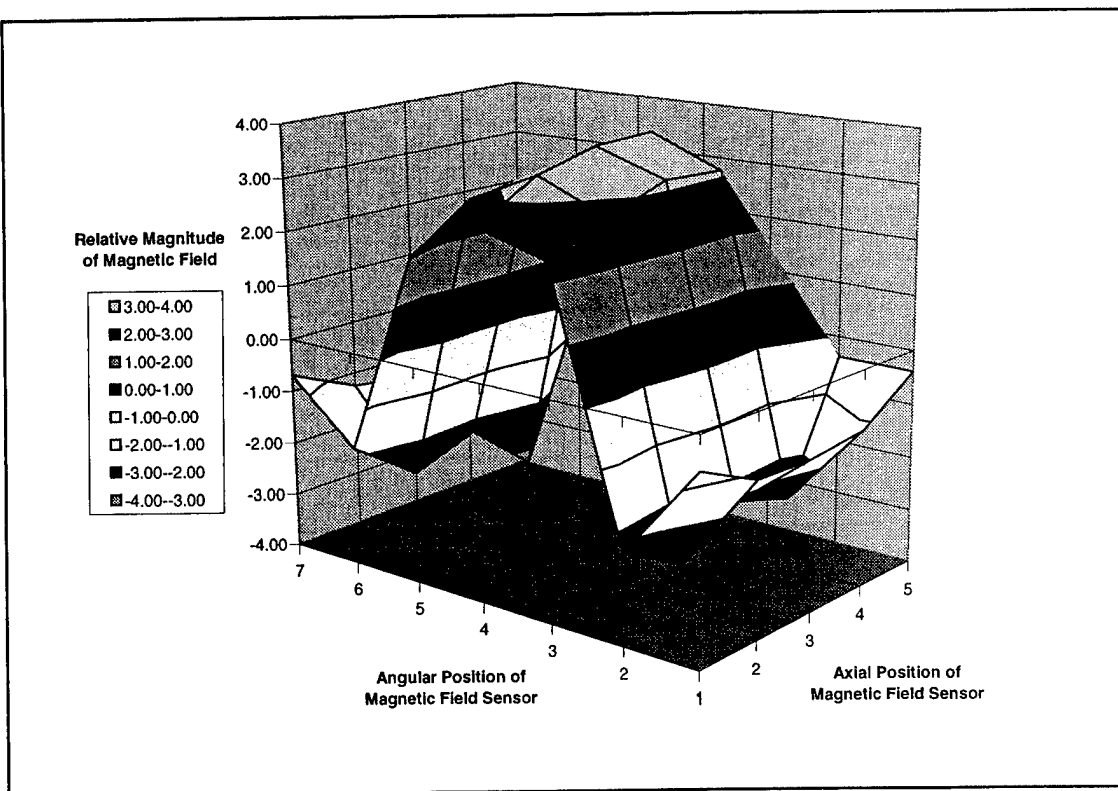

Figure 10. Relative Magnitude of Magnetic Field Across Panel #14
without the Panel in Place (Open)

12

When comparing the magnetic field profile across Panel #03 with Panel #14 (Figure 8 compared with Figure 10), it can be seen that each 3-D contour map has a similar characteristic profile. Maximum negative values occur along the bottom and top edge of the opening and the maximum positive values are centered in the opening. Due to cancellation effects of equal and opposite field contributions from the top and bottom edges of the panel's opening, one might initially anticipate little or no magnetic field to be present in the center of the panel's opening. Further analysis shows this is not true.

To better understand the analysis, it should be noted that the magnetic field loop sensor's active plane is parallel to the cylinder's radius (Figure 5). Therefore, magnetic flux *parallel* to this plane does not generate a signal. The sensor's "directionally dependent" signal only measures flux with a vector component orthogonal to its "active" plane. The fact that the sensor's signal may go to "zero" or change polarity implies nothing about the resultant magnitude of the total magnetic field, just the component that is normal to its "active" plane. [3]

Near the top and bottom edges of the panel the localized currents dominate the contribution of magnetic field which the magnetic field loop sensor tracks. The localized magnetic field is orthogonal to the loop sensor in those areas with the flux lines flowing perpendicularly through the sensor's active circular area, thus generating a maximum negative value. Although there are additional magnetic field contributions from the cylinder, the magnetic fields along these two areas of the panel are dominated by the currents flowing along the panel's edges.

In the center of the panel's opening, the localized currents along the edges of the opening no longer dominate the magnetic field contribution. Now, the "surface" magnetic field contributions from the current flowing along the entire length of the cylinder combine to create a new and larger peak value whose polarity has reversed. The polarity reversal is strictly a function of the loop sensor's orientation to the "surface" magnetic field. As the sensor position changes, the direction of the magnetic flux through it reverses. As a result, the sensor output decreases, goes through a null, and reverses polarity.

These 3-D plots indicate that in the areas where a panel is absent, the "surface" magnetic field "dips" into the panel's opening instead of remaining on the surface of the cylinder. The peak magnetic field areas, both positive and negative, indicate the locations where EM sensitive components and subsystems would be most susceptible to EM interference or damage from a magnetic field with a component orthogonal to the sensor's "active" plane.

Although Panel #14's 3-D plot is characteristically similar to Panel #03's plot, the overall magnitude has been reduced, i.e. the peak positive and peak negative magnetic field values are less. It is believed that as the current pulse travels the additional 22 feet from Panel #03 to Panel #14, diffusion effects have rearranged the surface current density in the aluminum cylinder to a more uniform distribution. The result is a lower amplitude waveshape.

It should also be noted that the 3-D profiles along the center, left edge of the panel openings (Positions 131 - 151) differ considerably. Panel #14's relative magnetic field value is approximately 70% higher than Panel #03's value. This may be attributed to Panel #14 having a more uniform current distribution around the panel's left edge due to its location 22 feet further down the aluminum cylinder from Panel #03's left edge. Bear in mind that four conductors connect the capacitor bank to the aluminum cylinder and Panel #03 was located between two of the current injection points. Also, the left edge of Panel #03 was only five feet from the capacitor bank connection while the left edge of Panel #14 was 26 feet away from the connection point.

To determine the shielding effects when the aluminum panel was screwed into place, a similar set of test shots was conducted with the sensor positioned at the various matrix positions of Panel #03 once the aluminum panel was screwed in place (38 screws per panel). The aluminum panel shielded the magnetic field sensor so well that the sensor only detected a very small signal that was dominated primarily by noise. A similar result occurred when a copper panel was secured in place. (A sample plot with the aluminum panel in place can be found in the bottom right insert of Figure 11 on page 15.)

3.2 Panel Material Effects

Figure 11 shows the relative magnetic field variations that result from changing the panel's material. The aluminum cylinder was subjected to current pulses of approximately 1.7 kA while three different panel configurations were investigated – air, brass screen and aluminum. For each shot, the magnetic field loop sensor remained in sensor position 351, i.e. centered in the middle of Panel #03 and even with the cylinder's skin surface.
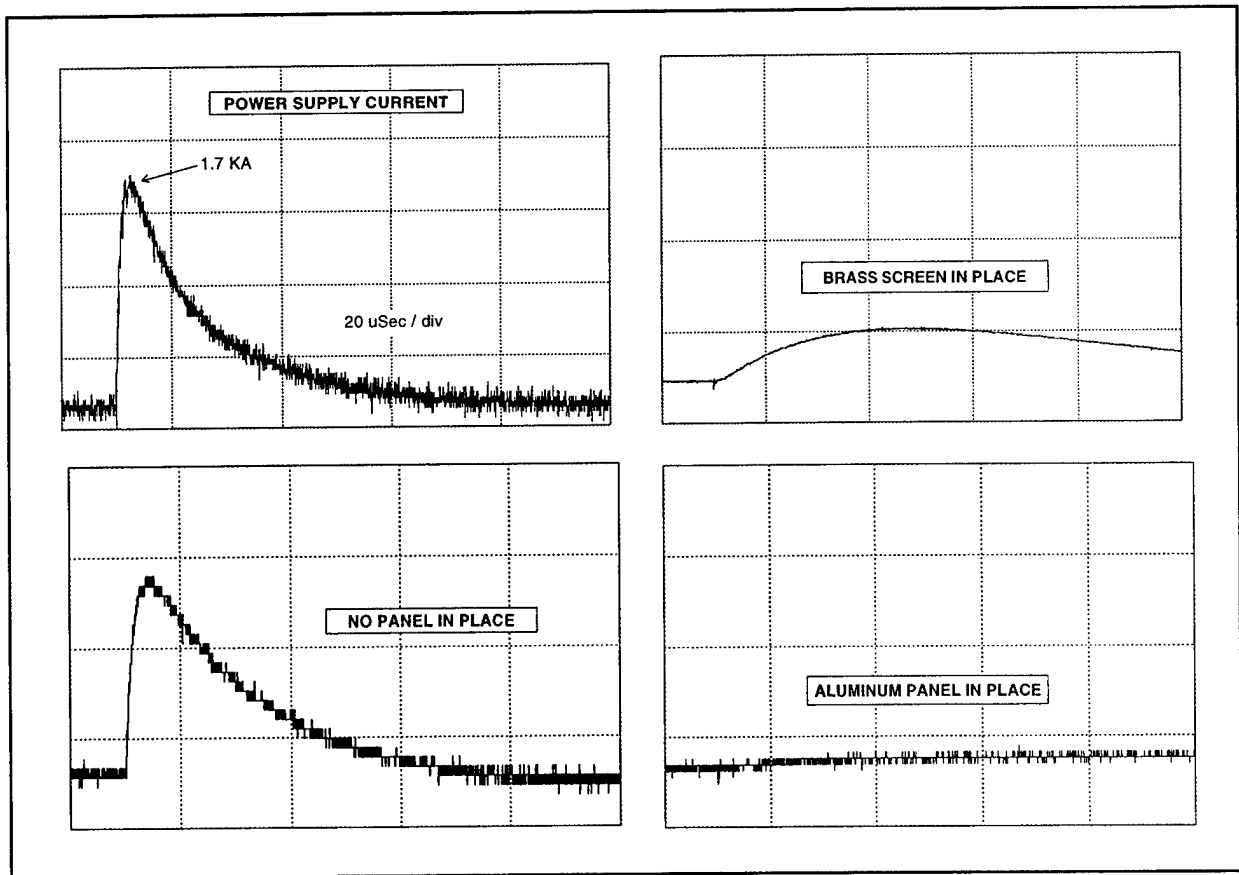

Figure 11. Relative Magnetic Field Variations at Panel #03 (Position 351)

Due to Various Panel Materials

As expected, with Panel #03 absent, there is a large aperture for the magnetic field to penetrate the aluminum cylinder and be detected by the magnetic field loop sensor. The magnetic field's characteristic curve tracks with the rise and fall of the capacitor bank's current pulse. When the opening is covered with a brass mesh screen (wire diameter $\approx$ 160 μm with a 200 μm x 200 μm square opening), the magnetic field amplitude is reduced by a factor of approximately 3.6. The peak magnetic field is delayed by about 40 μsec due to an impedance change ($L_{panel} = 0.646$ μH, $R_{panel} = 0.030$ Ω) and the low pass filtering effect of the wire mesh. Finally, when the aluminum panel is screwed into place ($L_{panel} = 0.611$ μH, $R_{panel} = 0.021$ Ω) the aperture is "sealed" magnetically, enhancing the shielding capacity of the cylinder to the extent that the magnetic field loop sensor is primarily sensing "noise" biased by a very weak magnetic field signal. [4]

3.3 Circuit Effects

A series of tests were conducted to estimate how the magnetic field resulting from the cylinder's surface currents might induce a current on a circuit internal to the cylinder. Initially, a 16 AWG, 28 strand, 24 foot long insulated wire (same as capacitor bank return wire) was attached to the cylinder's circular end plate closest to the capacitor bank. A machine screw and bolt anchored the wire about six inches radially inward from the cylinder's surface. The wire was laid parallel to the cylinder's surface and pulled taught to Panel #12 where it was bent 90° and reattached to the cylinder's outer surface. The total "area" of the rectangular loop created by the wire and the aluminum cylinder's surface was approximately 12 ft^2. A Pearson Current Transformer (Model #110A) encircled the wire to measure the current induced into the wire.

With only Panel #03 removed from the cylinder's surface and a current pulse of approximately 19 kA applied to the cylinder, a 6 amp current pulse was induced into the 24 foot wire. When the brass screen panel was secured onto the cylinder at position #03 and a similar 19 kA pulse applied, a 3 amp pulse was recorded (50% reduction). Finally, when the brass screen panel was replaced with the aluminum panel, the induced current pulse was reduced to approximately 2 amps (67% reduction).

To better understand the effects of cylinder openings and their locations relative to the induced current on the 24 foot long wire, a series of tests were run where various combinations of Panel #03 and Panel #12's locations were either open (no panel) or closed (aluminum panel in place). The capacitor bank current amplitude for this series of tests was approximately 14.5 kA. Table 1 shows the resulting induced current in the 16 AWG wire for the various panel configurations.

Table 1. Induced Current on Internal 24 Foot Long, 16 AWG Wire

Panel #03 Location	Panel #12 Location	Induced Current (A) in 16 AWG wire with I_{tot} = 14.5 kA
Open	Open	12.3
Open	Closed	7.0
Closed	Open	5.5
Closed	Closed	2.6

In general the more openings there are in the aluminum cylinder, the more the magnetic field penetrates into the cylinder. As the magnetic field penetration increases, the induced current on the 24 foot long wire also increases. This table also verifies that the closer the aperture is to the current source (simulated lightning strike point of attachment), the greater the induced current will be. For our simulated fuselage (32 feet long with a 38 inch diameter), being an additional 18 feet further away from the point of current injection reduced the induced current on the 24 foot long wire by 21%. For reference, Panel #03 was four feet away from the point of current injection.

Next, various resistors were added in series with the 24 foot long wire to see the effects on the induced current. Figure 12 shows a supply current of 15.5 kA and the resulting induced current traces when four different resistors were connected in series with the wire. Both Panel #03 and Panel #12 were open to generate the induced current traces.
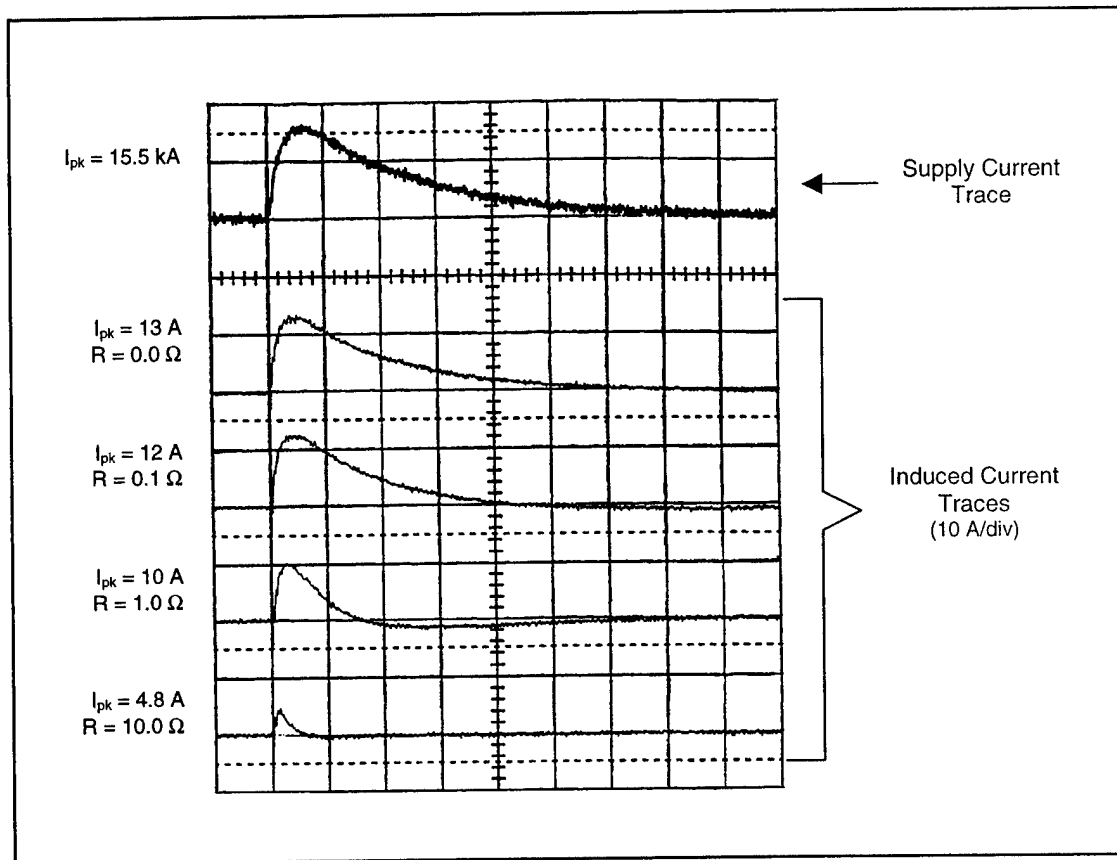
Figure 12. Induced Wire Currents with Various Resistors Connected in Series

Not only does the peak induced current value decrease as resistance increases but the induced current traces also dip below zero as the transmission line time constant changes with the various resistance values. This is to be expected as the system becomes less damped.

Finally, various capacitors were added in series with the 24 foot long wire to see the effects on the induced current. Figure 13 shows a supply current of 15.3 kA and the resulting induced current traces when three different capacitors are connected in series with the wire. Again, both Panel #03 and Panel #12 were open to generate the induced current traces.

When the capacitive components are added to the circuit, the energy rings between the inductance stored in the circuit's loop (≈ 12 ft^2) and the added capacitance. As the capacitance increases, the amplitude of the oscillations increase and the frequency decreases due to impedance and time constant changes.
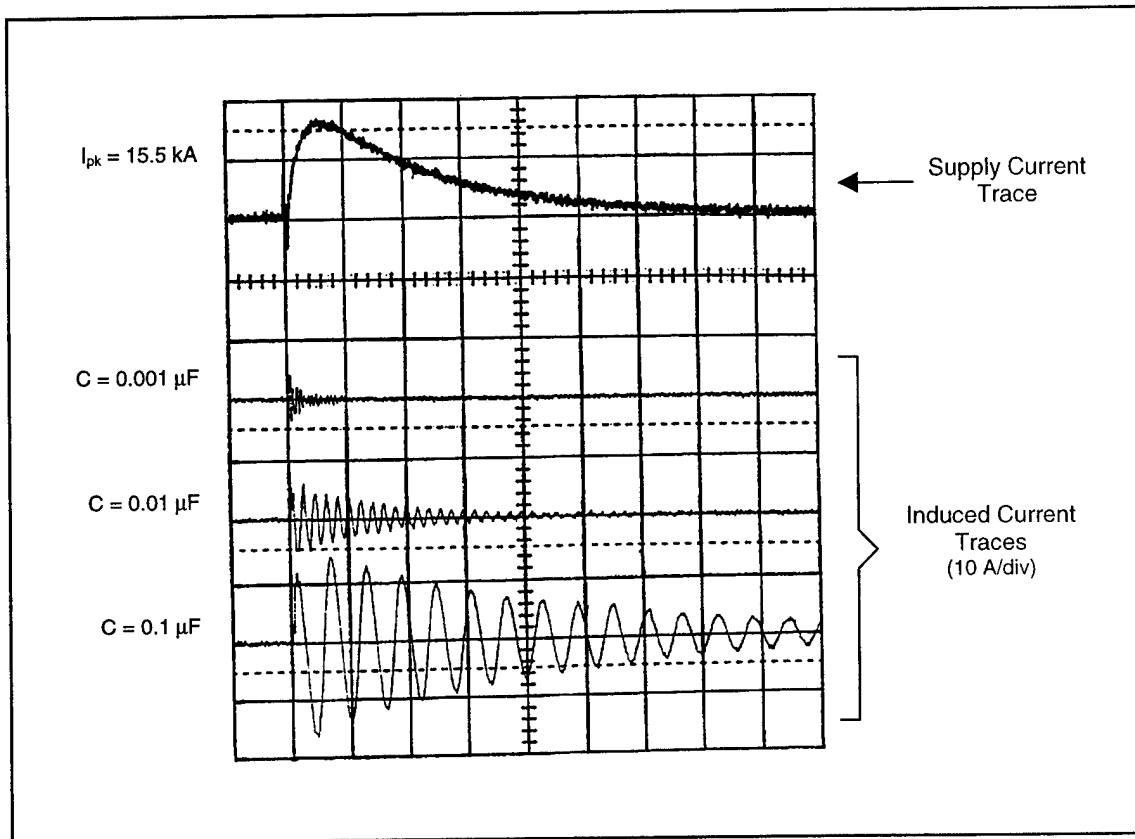
18

Figure 13. Induced Wire Currents with Various Capacitors Connected in Series

19

4.0 Conclusions

The purpose of this technical effort was to establish and verify the integrity of a test bed to simulate and monitor a low-level lightning strike on an aircraft fuselage. Once the power supply, aluminum cylinder, and associated circuitry were in place, instrumentation to monitor the capacitor bank current and related magnetic field was installed. With the necessary instrumentation in place, magnetic field variables such as location on the aluminum cylinder, position near a particular panel, and panel material effects were then investigated. A brief look at induced currents on internal circuits consisting of resistors and capacitors was also pursued.

The individual components of the test bed were robust throughout testing. The capacitor bank successfully fired more than 150 times. The aluminum cylinder and associated wiring connections never showed any signs of wear or fatigue. The mechanism developed to position the magnetic field loop sensor at the various grid positions repeatedly and accurately held the sensor at the appropriate location without influencing the magnetic field measurement. Due to the ability to "remotely" position the sensor when all panels were fastened to the cylinder, the sensor positioning mechanism substantially reduced the set-up time for each successive test. The instrumentation to monitor and store the current and magnetic field signals was also found to be very dependable. The ability to "replay" previous test shots was invaluable when comparing and contrasting various magnetic field profiles.

Although the characteristic shape of the magnetic field's 3-D profile for a particular panel was not predicted, it was generally consistent between the two locations tested. One difference in the magnetic field profiles was the peak magnitude fluctuations. The absolute values of both the positive and negative peaks on the panel closer to the capacitor bank were higher than the values for the panel that was further away from the capacitor bank. Also, the magnetic field at the "leading edge" of each panel differed. The panel farthest from the capacitor bank had significantly higher values by about 70%.

The shielding effects caused by various panel materials were as anticipated. With either the aluminum or copper panel in place, the shielding improved dramatically such that the

magnetic field internal to the cylinder was difficult to detect with the selected magnetic field loop sensor. A brass screen panel with a 160 μm wire diameter mesh reduced the internal magnetic field by a factor of almost four and also caused a time delay of approximately 40 μsec due to low-pass filtering effects.

Using a 24 foot long wire internal and parallel to the cylinder to form a circuit, induced currents were monitored as panel openings were changed. The results confirmed that the closer to the source and the more openings in the cylinder, the larger the induced current on the wire. As various resistors and capacitors were added to the circuit, the induced current profile changed based on the value and type of electrical component. Higher resistances resulted in current traces with smaller peak values and a shorter time constant. Higher capacitances resulted in larger oscillations at lower frequencies.

Recommendations for future investigations include generating additional 3-D plots at other locations along the aluminum cylinder. To further enhance these plots, the present grid matrix of 35 points should be at least doubled to better define where magnetic field peaks and zero-crossings occur. Such plots would greatly aid the development of computer modeling for such systems by providing invaluable data for verification of the models. Additional panel materials should be investigated to include wire mesh of different diameter wire and composite materials as well. Finally, more complex electrical circuits and systems located internal to the cylinder should be analyzed to determine their ability to survive electromagnetic pulses resulting from high-current pulse discharges.

5.0 References

1. L. C. Walko, D. L. Schweickart, J. Gruden, G. Tsai Li, B. Jarupan, S. A. Sebo, "Full Scale Lightning Generation Techniques for Aircraft Susceptibility Evaluations," Proceedings of the 32nd Intersociety Energy Conversion Engineering Conference, Honolulu, HA, 1997, vol. 1, pp. 359-363

2. L. C. Walko, D. L. Schweickart, J. Gruden, G. Tsai Li, B. Jarupan, S. A. Sebo, "Full Scale Lightning Test Technique: Cylinder Current Investigation," Proceedings of the 10th International Symposium on High Voltage Engineering, Montreal, September 1997, vol..5, pp. 269-272.

3. C. R. Paul, S. A. Nasor, "Introduction to Electromagnetic Fields, McGraw-Hill Book Co.: New York, 1982

4. F. W. Grover, "Inductance Calculations," I.S.A., Dover, 1973